International Journal of Emerging Research in Engineering, Science, and Management
Vol. 5 | Issue 2 | pp. 01-22 | Apr-Jun 2026.
www.ijeresm.com | eISSN – 2583-4894
Received: 28 Dec 2025 | Revised: 06 Apr 2026 | Accepted: 18 Apr 2026 | Published: 26 Apr 2026

Enhanced Prediction of Chronic Kidney Disease Based on an Integrated Framework of High-Dimensional Medical Image Data and Deep Learning

[1]M. Naresh, [2]M. V. Nageswara Rao, [3]D. Venkat Reddy,
[4]Koiloth SRS Jyothsna, [5]Namburi Dhana Lakshmi, [6]Nanduri Srinivas

[1]Associate Professor, Department of ECE, Matrusri Engineering College, Saidabad, Hyderabad, India.
nareshmuddamalla@matrusri.edu.in, ORCID ID: 0000-0002-3631-1981
[2]Associate Dean-Academics, GMR Institute of Technology, Razam, Andhra Pradesh 532127, India.
nageswararao.mv@mgit.edu.in, ORCID ID: 0000-0003-3590-3501
[3]Professor, Department of ECE, Mahatma Gandhi Institute of Technology, Gandipet, Hyderabad, Telangana - 500075, India. dvenkatreddy_ece@mgit.ac.in, ORCID ID: 0009-0000-5962-1993
[4,5]Assistant Professor, Department of ECE, Chaitanya Bharathi Institute of Technology, Gandipet, Hyderabad, Telangana - 500075, India.
[4]jyothsna_ece@cbit.ac.in, ORCID ID: 0000-0001-6074-9433
[5]dhanalakshmi_ece@cbit.ac.in, ORCID ID: 0000-0002-4532-0978
[6]Associate professor, Department of Mathematics, R K College of Engineering, Kethana Konda, NTR District, Andhra Pradesh, India. sri.srinivas83@gmail.com, ORCID ID: 0009-0006-7862-6603

Corresponding Author: M. Naresh

Abstract: Chronic kidney disease (CKD) is characterized by progressive kidney damage and is a rapidly growing global health concern. CKD significantly increases morbidity and mortality risk. One way to lower the CKD mortality rate is to diagnose and treat patients early. Early detection of CKD remains challenging for medical practitioners. By integrating state-of-the-art deep-learning (DL) methods with high-dimensional medical image data, the proposed model enhances CKD prediction while addressing challenges related to data quality and scalability. Pre-processing, feature extraction, feature selection, and classification are the four stages of the proposed framework. The three models that extract the essential features are Inception-V3, ResNet-50, and VGG-16. In order to choose the best features and minimize problems caused by feature dimensionality, an upgraded version of the particle swarm optimization method (UPSO) is introduced during the feature selection step. Then, a deep capsule model combined with a depth-wise convolutional network is used for classification. The last step in improving CKD prediction is hyperparameter optimization, namely the Crayfish Optimization Algorithm (COA). Using performance metrics such as accuracy, precision, recall, F1-score, and specificity, the proposed technique is validated using benchmark CT kidney and retinal image datasets. The proposed model achieves an accuracy of 99.72% by integrating hybrid MMG–CLAHE preprocessing, multi-backbone transfer learning feature extraction (Inception-V3, ResNet-50, VGG-16), UPSO-based feature selection, and a depth-wise convolutional capsule classifier optimized using COA for CKD prediction.

Keywords: Chronic kidney disease, Deep learning, Medical image analysis, Transfer learning, Capsule network, Crayfish optimization algorithm.

1 INTRODUCTION

Chronic kidney disease is characterized by diminished kidney function. CKD causes a significant number of deaths worldwide. Approximately 10–13% of the global population has CKD. Diagnosing CKD is expensive and may require lifelong therapy [1][2]. Retinal vascular changes such as venular dilatation and arteriolar constriction have been associated with CKD in previous studies [3]. Public and primary care settings often employ digital retinal photography, a non-invasive technique for screening for diabetic retinopathy and other eye conditions. CKD is typically classified into five stages based on glomerular filtration rate (GFR), ranging from Stage 1 to Stage 5 (end-stage kidney disease). CKD affects millions of people worldwide and contributes significantly to global mortality [4]-[6]. Urine and blood samples must be collected in order to commence the evaluation of kidney function. Creatinine is a substance in the blood that is used to calculate the glomerular filtration rate (GFR). The variables used to assess CKD were test results, sex, and age [7]. Three major strategies, including pre-processing, feature selection, and classification, have contributed to successfully completing the CKD diagnosis. Multiple technologies, like deep learning and machine learning, have been invented for the diagnosis of CKD.

International Journal of Emerging Research in Engineering, Science, and Management
Vol. 5 | Issue 2 | pp. 01-22 | Apr-Jun 2026.
www.ijeresm.com | eISSN – 2583-4894
Received: 28 Dec 2025 | Revised: 06 Apr 2026 | Accepted: 18 Apr 2026 | Published: 26 Apr 2026

Some of the common DL methods are CNN, RNN, and GRU (gated recurrent units). Since CNN is a deep hierarchical learning method, combining CNN with LSTM architecture has been reported to improve CKD classification accuracy in previous studies [8]. Previous studies have demonstrated the effectiveness of deep learning in disease diagnosis, healthcare prognosis, and personalized treatment. However, there is still a lot of work to be done in terms of data quality, interoperability, ethical considerations, regulatory compliance, and scalability [9][10]. To predict CKD in patients, three-dimensional convolutional neural networks (CNNs) are trained using volumetric medical imaging data. Various DL architectures were presented for CKD prediction, which mainly rely on either feature extraction or feature selection methods [11].

2D convolution proceeds on 2D data and generates a 2D outcome, but most medical imaging datasets used in this study consist of 2D image slices. Predicting CKD might benefit from a 3D CNN's ability to perform convolution in three directions. Nevertheless, the 3D CNN-based CKD grade classification has not been the theme of numerous studies, which may be attributed to the computationally intensive character of the technique [12][13]. The EO-LWAMCNet model is suggested as a reliable approach to predicting the long-term medical status of a patient with heart or renal disease. A gateway is used to transmit each data point that an embedded sensor in the patient's body acquires to the cloud [14]-[16].

1.1. Problem Statement and Motivation

The merging of disparate healthcare data sets into cohesive systems is at the heart of large-scale medical image data and DL integration. Clinical decision-making, diagnostic accuracy, and treatment plan personalization are all aided by this integration. Researchers have already proved that DL helps with cancer detection, healthcare prediction, and individualized medicine. Still, there are challenges to overcome, like creating scalable solutions, achieving interoperability, addressing ethical concerns, and managing regulatory compliance. Still, there's a lot of room for enhancement in healthcare and patient care when deep learning and high-dimensional medical image data work together. To predict CKD from data, this study will employ sophisticated DL procedures. The objectives of the suggested approach are,

- To remove unwanted noise and enhance the contrast of the input image, mean, median, and Gaussian filtering, and adaptive histogram equalization (AHE) are employed correspondingly.
- To extract the related features from the pre-processed image, transfer learning methods, including Inception-V3, ResNet-50, and VGG-16, are utilized.
- To select optimal features and to reduce the feature dimensionality, an updated Particle Swarm Optimization (PSO) algorithm is employed.
- To accurately detect chronic kidney disease, an advanced DL approach, namely a depth-wise convolutional network with a deep capsule model with high-dimensional image data, is developed.
- To improve prediction efficiency and adjust classifier constraints and weights, an effective COA is employed.

The main contributions of this study are summarized as follows:

1. A hybrid MMG–CLAHE preprocessing pipeline is developed to enhance contrast and suppress noise in high-dimensional kidney and retinal medical images.
2. A multi-backbone transfer learning feature extraction strategy integrating Inception-V3, ResNet-50, and VGG-16 is proposed to capture complementary spatial and semantic representations.
3. An improved particle swarm optimization algorithm is employed for optimal feature selection and dimensionality reduction.
4. A hybrid classification framework combining depth-wise convolutional networks and deep capsule networks is introduced to preserve hierarchical spatial relationships during CKD prediction.
5. The crayfish optimization algorithm is utilized for hyperparameter tuning to improve convergence stability and prediction accuracy.
6. The proposed framework is validated using CT-kidney and multicenter retinal KIDS datasets with patient-level data splitting, k-fold cross-validation, ablation analysis, and statistical significance testing.

The rest of this paper is arranged as follows: Section 2 offers some relevant papers based on CKD prediction. The proposed method is summarized in Section 3. The results and a discussion are presented in Section 4. The suggested work's conclusion is illustrated in Section 5.

2 Related Work

To detect and anticipate CKD, V. Singh et al. [1] introduced a DL-based DNN method. Iteratively applying the settings that had been fine-tuned using a neural network allowed the model to reduce prediction errors. Maximizing important features was achieved by this strategy using Recursive Feature Elimination (RFE). The most important values were packed cell volume, specific gravity, hemoglobin, serum creatinine, albumin, red blood cell count, and hypertension. After applying the selected features, classification performance improved compared with other machine learning algorithms such as KNN, SVM, Random Forest, Logistic Regression, and Naïve Bayes. The study used the UCI repository dataset for CKD classification.

International Journal of Emerging Research in Engineering, Science, and Management
Vol. 5 | Issue 2 | pp. 01-22 | Apr-Jun 2026.
www.ijeresm.com | eISSN – 2583-4894
Received: 28 Dec 2025 | Revised: 06 Apr 2026 | Accepted: 18 Apr 2026 | Published: 26 Apr 2026

The small dataset size that the DL model used was one of its drawbacks. The HMANN model was designed by F. Ma et al. [17] for the analysis and classification of CKD in its early stages using the IoMT platform. SVM and Multilayer Perceptron (MLP)-associated backpropagation techniques were used together in the model to determine CKD. It was reported that the HMANN model achieved 97.5% accuracy on the CKD dataset and reduced prediction time compared with conventional machine learning models. However, the model lacked sufficient predictive features for broader generalization.

To diagnose kidney disease, V. Nayarasan et al. [18] developed a deep K-Net model based on CNN architecture with multiple convolutional layers. To make the diagnosis of DL-based CKD, kidney image data were extracted from the TCIA dataset. Metrics such as accuracy, precision, recall, and F1-score were used to evaluate the model performance. The efficiency and accuracy of the model are the major advantages of using this method. One of the biggest issues with this approach was the high computational complexity of the model. The performance of the CNN model trained on an open-source dataset in detecting CKD in the input image was reported by B.S. Lakshmi et al. [19]. In this case, the classifier model performs well when it comes to making accurate predictions by taking advantage of a convolutional layer, a max pooling layer, and many activation functions. Data augmentation, splitting, normalization, and resizing were performed during the preprocessing stage. Their model performance was evaluated using accuracy, precision, recall, and F1-score.

In their study on CKD disease prediction, C. Yun et al. [20] developed a Stacked Ensemble that utilized meta-learners such as naïve Bayes, k-nearest neighbor (KNN), and logit-boost. Data obtained from a public source, namely the UCI ML repository, was used to test numerous performance metrics, including accuracy, precision, sensitivity, F-measure, and false positive rate. Because it relies on classical machine learning methods for CKD prediction, this model shows limited robustness. A Graph Neural Network (GNN) deep learning model and a tabular data model were proposed by P.K. Rao et al. [21] for the recognition of CKD. The GNN model examined graph-structured data to discover intricate associations among patients and their health conditions, whereas the table-based approach meticulously preserved patient-specific data in a structured tabular format. There was extensive testing of the fusion model, tabular data model, GNN model, and baseline model employing metrics including recall, F1-score, and accuracy. This method achieved a 95.089% success rate on the India UCI ML Repository dataset. Reduced disease prediction accuracy was a drawback of this approach.

A DNN model has been suggested by H. Kriplani et al. [22] as a means of CKD detection. The dataset was classified using a DL technique based on the UCI ML repository dataset, and a 97% success rate was achieved in forecasting the occurrence or lack of CKD. Various other algorithms were used to cross-validate the DL model. With a kappa value of 0.955 and an RMSE of 0.121, the deep neural network model attained 97.7 percent accuracy. One drawback of this approach was the decreased precision it achieved. Most existing models achieve accuracy values between 90% and 95% after examining the summary of related articles on CKD prediction. However, those models have several drawbacks, such as limited datasets, computational complexity, and decreased robustness. The suggested method has been created to overcome these drawbacks. The next section provides a full overview of the suggested technique.

3 Proposed Methodology

To improve CKD prediction, the proposed study combines high-dimensional medical image data with advanced deep learning algorithms. ML and DL models for CKD recognition have been widely studied; however, their predictive accuracy and computational efficiency are often limited because they rely on either feature extraction or feature selection independently. The novelty of this work comes from several important contributions. Unlike existing CKD prediction models that rely on single backbone architectures or tabular clinical datasets, the proposed framework integrates multi-backbone feature extraction with capsule-based classification and metaheuristic optimization on multimodal medical image datasets.

This paper uses the UPSO method for dimensionality reduction and feature selection. This preserves computational efficiency without sacrificing predictive performance. To improve classification accuracy, a deep capsule model combined with a depthwise convolutional network (DW-Conv) is developed. This hybrid model maintains spatial relationships between features using capsule networks and captures spatial hierarchies through depth-wise convolutions. The proposed model incorporates the COA as a metaheuristic optimization technique to optimize classifier weights and parameters for improved prediction accuracy and convergence. Tested on benchmark CT kidney and retinal image datasets, the proposed approach outperforms existing models for CKD prediction and achieves higher accuracy. This demonstrates the effective integration of deep learning architectures, optimization approaches, and transfer learning techniques. This study addresses major issues in CKD prediction, including data quality, feature redundancy, and computational complexity. The proposed method provides a more accurate and scalable framework for early CKD detection, which may assist physicians in clinical decision support.

International Journal of Emerging Research in Engineering, Science, and Management
Vol. 5 | Issue 2 | pp. 01-22 | Apr-Jun 2026.
www.ijeresm.com | eISSN – 2583-4894
Received: 28 Dec 2025 | Revised: 06 Apr 2026 | Accepted: 18 Apr 2026 | Published: 26 Apr 2026

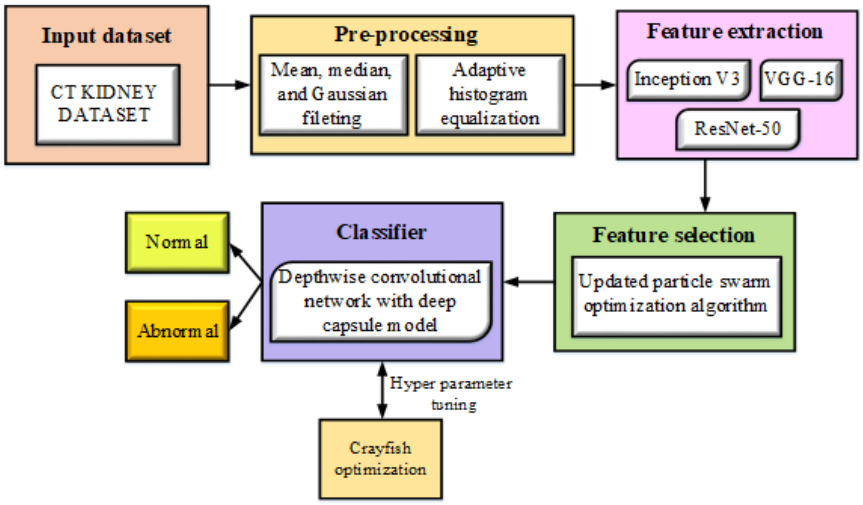

Fig. 1. Overall workflow architecture

The first stage uses a two-level approach for preprocessing the input data. Publicly available CT kidney and retinal image datasets were used for this study. The preprocessing stage includes mean filtering [23], median filtering [24], and Gaussian filtering [25]. In addition, CLAHE is being used to reduce unwanted noise and improve contrast. Then, three transfer learning models, namely Inception-V3, ResNet-50, and VGG-16, are used to extract discriminative features from high-dimensional image data. The feature selection approach is an enhancement of the PSO methodology that reduces feature dimensionality and identifies the most effective features. Finally, a deep capsule network combined with a depth-wise convolutional network is applied for CKD prediction. The Crayfish Optimization Algorithm is used to optimize model parameters and weights. The structural design is shown in Fig. 1.

3.1. Data Pre-processing Techniques

3.1.1. Data Pre-processing

To guarantee good quality input data and maximize model performance, a two-stage pre-processing is performed. A hybrid filtering strategy is developed that removes noise from medical images without structural information loss or distortion. This technique integrates the mean, median, and Gaussian filters. The feature extraction method uses Inception-V3, ResNet-50, and VGG-16 to provide a comprehensive representation of CKD-related patterns. Using an updated Particle Swarm Optimization method for optimization preserves uniformity across input data while reducing dimensionality and retaining critical information. Normalization of the retrieved high-dimensional features further ensures this. The suggested method is both scalable and applicable to real-world CKD detection because of its robust preprocessing pipeline, which ensures clearer images, consistent features, and computational efficiency. Preprocessing is performed in two stages using adaptive histogram equalization and MMG filtering. The approaches are briefly described in the following section.

3.1.2. MMG Filtering

A hybrid filtering technique called MMG gathers mean, median, and Gaussian filtering. Hybrid MMG filtering is employed to overcome the limitations of individual filtering algorithms. One drawback of mean filtering is that it can produce hazy images due to the distortion of pixel intensities by outlier pixels. When it comes to median filtering, removing high-density impulsive noise is challenging. These limitations are addressed using the proposed MMG filtering approach. The primary contribution of mean filtering is to suppress low-level noise and minimize the luminance fluctuations in the background without affecting the vessel structures. The median filter intends to remove small artifacts and impulse noise. It can preserve vessel edges. The Gaussian filter enhances spatial smoothing and reduces high-frequency noise.

Applying Gaussian, median, and mean filters to the input image uses a 3 × 3 kernel matrix. To construct a single image, compute the output vectors for the same pixels across the input images and combine them using MMG. The output vector of pixel values can be calculated to achieve normalization, as demonstrated below.

$$MMG_{p,q} = 255 \times \frac{\sqrt{(Mean_{p,q})^2 + (Median_{p,q})^2 + (Gaussian_{p,q})^2}}{Max(MMG_{p,q})} \quad (1)$$

where, MMG represents the filter's softened new image, the maximum pixel value produced by the output vector is represented as $MMG_{p,q}$.

International Journal of Emerging Research in Engineering, Science, and Management
Vol. 5 | Issue 2 | pp. 01-22 | Apr-Jun 2026.
www.ijeresm.com | eISSN – 2583-4894
Received: 28 Dec 2025 | Revised: 06 Apr 2026 | Accepted: 18 Apr 2026 | Published: 26 Apr 2026

3.1.3. Adaptive Histogram Equalization

Histogram Equalization (HE) is one of the most fundamental methods for image enhancement [26]. One variant of HE is Adaptive Histogram Equalization, or AHE. In this method, surrounding pixels are used to improve local contrast within the selected region. After that, local histogram statistics are used to calculate the sliding window's grey value distribution. Then, the central pixels' HE transfer function is determined. In the proposed pre-processing pipeline, AHE and CLAHE are applied to enhance image contrast by redistributing pixel intensities. A key parameter in this process is the filter radius, which defines the local window size used to compute histograms. The default window size is 8x8 pixels, a commonly used parameter in medical imaging that provides high contrast without losing fine details. The window size is adaptively determined based on the image resolution and feature distribution to balance local contrast enhancement and computational efficiency. The clip limit is set as 2.0, and the tile size is fixed as 8 × 8. It is mainly used to improve vessel-background contrast with reduced noise amplification. It is widely used in medical image processing as it enhances the visibility of thin vessels and low-contrast regions without including artificial edges.

Overlapping windows are applied with a 50% stride to ensure a smooth transition between adjacent regions and avoid abrupt changes in intensity in the enhanced images. The size of the window is scaled proportionately so that too high local contrast enhancement of larger medical images may not be introduced as an artifact. By adapting to various image settings, our method makes contrast improvement efficient, ensuring that CKD-related characteristics stand out while avoiding overly large distortions. Contrast-Limited Adaptive Histogram Equalization, or CLAHE, is the transfer function that is utilized. Lastly, the process of utilization of multilayer histograms is described for the analysis of AHE and CLAHE. A comprehensive overview is provided by Algorithm 1.

Algorithm 1: Overview of AHE and CLAHE
Need: image i , filter radius r
Confirm: Managed image output i^{out}
Procedure $AHE(i, r)$
for (p, q) in $i$do
Calculate histogram window $H_{p,q}$
Level histogram $H_{p,q}$
if AHE then
allocate changed grey value $i_{p,q}^{out} \leftarrow f(i_{p,q})$
else if CLAHE then
calculate clipped histogram $\bar{H}_{p,q}$
assign converted grey value $i_{p,q}^{out} \leftarrow \bar{f}(i_{p,q})$
end if
end for
end Process

The local processing window can extend beyond the image bounds when using AHE and CLAHE, which may cause edge effects. To avoid artifacts and make sure the contrast enhancement is smooth around the edges, this is done. To avoid jarring changes in brightness or contrast, the picture is proportionately cropped at the edges, reflecting the pixel values in the process. The stability of histogram calculations is ensured by replicating the nearest pixel values at the boundary to fill missing sections. Without padding, the local histogram window may be truncated at the image boundary, limiting contrast enhancement to only valid pixels. To avoid distortions and guarantee artifact-free picture pre-processing for CKD feature extraction, these algorithms make sure that edge pixels receive adequate contrast changes.

3.2. Feature Extraction

The suggested method used three models, Inception V3, ResNet-50, and VGG-16, to extract relevant properties from large data sets. High-dimensional image features are extracted by these models, and the features that are extracted are assessed at various stages of the model. Benefits of using high-dimensional image data for feature extraction include increased efficacy and quality of extracted structures.

3.2.1. Inception V3

It has 48 layers and is a pre-trained CNN model [27]. It can learn complex patterns and discriminative features from medical images. A key advantage of Inception-V3 is its ability to process high-dimensional medical image data and handle images of varying sizes and resolutions. There is a difference in the quality, resolution, and size of the medical images. This model helps reduce overfitting and improves the network's ability to generalize across varying image scales.

International Journal of Emerging Research in Engineering, Science, and Management
Vol. 5 | Issue 2 | pp. 01-22 | Apr-Jun 2026.
www.ijeresm.com | eISSN – 2583-4894
Received: 28 Dec 2025 | Revised: 06 Apr 2026 | Accepted: 18 Apr 2026 | Published: 26 Apr 2026

$$A_y = \begin{bmatrix} A_{11} & \cdots & A_{1N} \\ A_{21} & \cdots & A_{2N} \\ A_{M1} & \cdots & A_{MN} \end{bmatrix} * \begin{bmatrix} B_{11} & \cdots & B_{1N} \\ B_{21} & \cdots & B_{2N} \\ B_{M1} & \cdots & B_{MN} \end{bmatrix} = \sum_{j=0}^{M-1} \sum_{k=0}^{N-1} A_{(N-1),(M-k)} B_{(j+1),(k+1)} \quad (2)$$

The dimensions of the output layer are reduced and trimmed to avoid overfitting issues. A softmax classification layer is included for multi-class classification, along with initializing the classification layer's weights.

$$F(y) = MAX(0, y) \quad (3)$$

$$X_K \sim u\left(\frac{-1}{\sqrt{n}}, 1/\sqrt{n}\right) \quad (4)$$

From the above equation, the uniform distribution lies between the breaks of $-b$and c is represented by $u(-b, c)$, the previous layer size is represented by$n$and the weight parameters of the CNN with iteration K is denoted by X_K. The structural design of Inception-V3 is depicted in Fig. 2.

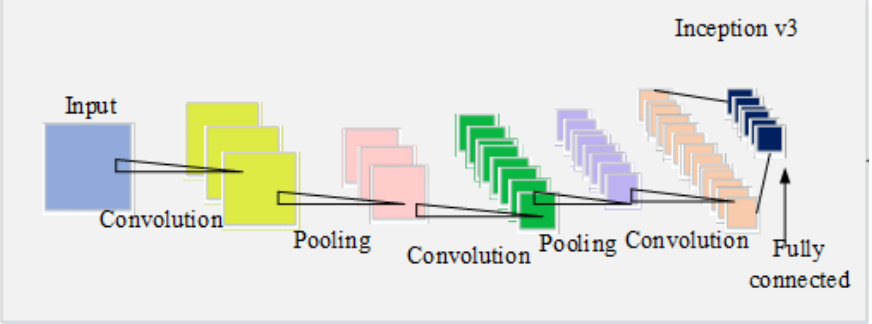

Fig. 2. Inception-V3

3.2.2. ResNet-50

M. Elpeltagy and H. Sallam [28] describe the 50-layer residual network ResNet-50 as a widely used model for image recognition and classification tasks. It was successfully applied in the ImageNet Large Scale Visual Recognition Challenge (ILSVRC) and mitigates gradient degradation while improving training efficiency. ResNet-50 was originally trained to classify images into 1000 object categories in the ImageNet database. The ResNet-50 architecture specifies convolutional layers with residual connections that improve feature learning efficiency. The final convolutional layer outputs high-level feature representations that are used for downstream classification. The notation “k” designates the convolutional filter size used within the residual blocks. A layer with 1000 fully connected neurons is called FC 1000. The term “n classes” refers to the number of output classes. The architecture of ResNet-50 is shown in Fig. 3.

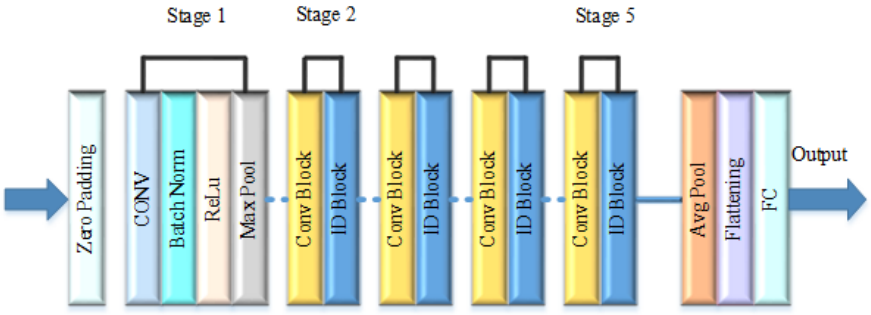

Fig. 3. ResNet-50 architecture

3.2.3. VGG-16

VGG-16 [29] consists of 16 weight layers, including convolutional and fully connected layers. It includes thirteen convolutional layers and three fully connected layers. Each convolutional layer uses a 3 × 3 kernel. The VGG-16 model extracts hierarchical feature representations from medical images. The three FC layers of the VGG 16 model have different depths; the final fully connected layer contains 1000 output neurons, whereas the first two FCs have a channel size of 4096. The softmax layer produces class probability outputs for classification. The architecture of VGG-16 is shown in Fig. 4.

International Journal of Emerging Research in Engineering, Science, and Management
Vol. 5 | Issue 2 | pp. 01-22 | Apr-Jun 2026.
www.ijeresm.com | eISSN – 2583-4894
Received: 28 Dec 2025 | Revised: 06 Apr 2026 | Accepted: 18 Apr 2026 | Published: 26 Apr 2026

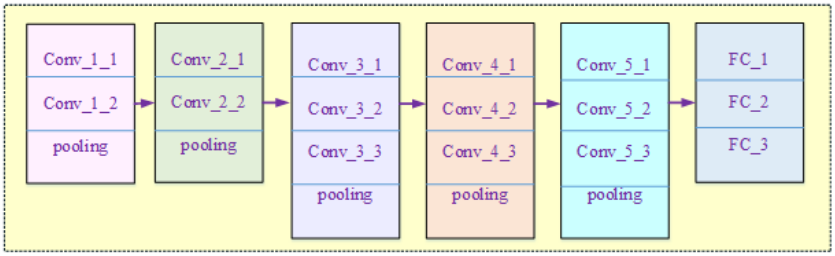

Fig. 4. VGG-16 Architecture

3.3. Feature Selection

To create an effective prediction model, irrelevant features are eliminated through effective feature selection. Irrelevant features increase computational cost and contribute to dimensionality issues. An improved PSO method is used in this work to extract the optimal attributes.

3.3.1. Updated particle swarm optimization algorithm

This section presents modified variants of the PSO technique [30]. The improved PSO-HBF variant is used to enhance optimization performance. In fundamental PSO, three collections of courses are delineated:

(1) initial population i, in the size of the problem measurement, D; $Z^{i,it} = \left[z_1^{i,it}, z_2^{i,it}, \ldots . z_D^{i,it}\right]$

(2) the ideal state known by the particle $i, pbest^{i,it}$, and

(3) the ideal state amongst all particles is $Gbest^{it}$.

Each time the evolution process iterates, all these vectors are changed to have the index it. The particles in PSO employ social behavior since every particle i, use the information of $pbest^{i,it}$ and $Gbest^{i,it}$ to update its position. The recommended informed PSO-HBF system, $Z^{i,it+1}$ designates a better solution than $Z^{i,it}$ old particle is substituted by an original particle, which can be described as,

$$Z^{i,it+1,pso} = \begin{cases} Z^{i,it} iff(Z^{i,it}) \leq f(Z^{i,it+1}) \\ Z^{i,it+1} iff(Z^{i,it+1}) \leq f(Z^{i,it}) \end{cases} \quad (5)$$

After informing the place of the element, i.e. $Z^{i,it+1,pso}$, the HBF tactic is executed for the target particle. To execute the HBF tactic, an initial random step is produced with the choice to employ dissimilar kinds of arbitrary values. It employs two kinds of limitations $T$and$t$, where Tsignifies the extent of the growth procedure while t signifies the number of iterations.

3.4. Classifier

The use of a hybrid DW-Conv and deep capsule network (DCN) classifier is the main distinctive aspect of the proposed methodology. The main goals of the depth-wise convolution algorithm are to enhance performance, reduce training time, and decrease processing costs. This equilibrium enables the model to focus on important features for CKD classification. On top of that, unlike conventional CNNs, deep capsule networks preserve spatial relationships between features more effectively [31]. There are two components to the separable convolution: the depth-wise (DW) and the point-wise convolutions (PWC). For DW, all channels of the original feature maps use the same filter. DW is represented by equation (6).

$$K(l,m,n) = \sum_{v=1}^{m} \sum_{v=1}^{m} m(v,v,n) \times k(l+v-1, m=v-1, n) \quad (6)$$

where N indicates DW kernels of extent $n \times n \times n \times m_{in}$. The m filter is used on the frequency in I to create n_{th} canal of riddled outcome feature map G. By constructing a linear gathering of the output of a DWC using a 1 X 1 convolutional, a PWC generates new features.

$$p(x,y,z) = \sum_{i=1}^{m_{in}} K(x,y,z) \times V(i,o) \quad (7)$$

The extent of a 1 × 1 convolutional kernel is $1\times 1 \times m_{in} \times m_{out}$. The channel has changed over filtering m with convolutional roles$k \times k(k > 1)$.

$$F_{ds} = k^2, m_{in}, h, w + m_{in}, m_{out}, h, w \quad (8)$$

International Journal of Emerging Research in Engineering, Science, and Management
Vol. 5 | Issue 2 | pp. 01-22 | Apr-Jun 2026.
www.ijeresm.com | eISSN – 2583-4894
Received: 28 Dec 2025 | Revised: 06 Apr 2026 | Accepted: 18 Apr 2026 | Published: 26 Apr 2026

A 1 × 1 convolution is computed in the point-wise convolution stage. The conventional convolutional and depth-wise separable convolutional levels of difficulty are resolved by subsequent factors:

$$\eta = \frac{R_{ds}}{R_{std}} = \frac{k^2 m_{in} hw + m_{in} M_{cout} hw}{k^2 m_{in} m_{out} hw} = \frac{1}{m_{in}} + \frac{1}{k_2} \tag{9}$$

The factor is moderately great of m, the issue is about η equal to $\frac{1}{k_2}$. The likelihood of an entity's existence is represented by the lengths of these vectors. These representational restrictions are mostly the result of CNNs, and more specifically, their pooling layers. As a consequence, in capsule networks, those layers are modified utilizing an additional appropriate approach called "routing by agreement". The outputs created by this criterion are delivered to the original capsules in the next layer. However, the coupling powers change. As v_i is the yield of the shell i, it's predication of the parent shell j is calculated as follows,

$$v_{j|k} = X_{jk} v_k \tag{10}$$

The capsule output prediction path at the higher level was intended by the j^{th} shell at the lower layer is $v_{j|k}$, as well as the weighting matrix to be learned in the backward pass is X_{jk}. The succeeding condition exploits the softmax role to calculate coupler coefficients c_{ij}. Fig. 5 displays the suggested classifier scheme.

$$b_{kl} = \frac{exp(c_{ij})}{\sum k \, exp(b_{ik})} \tag{11}$$

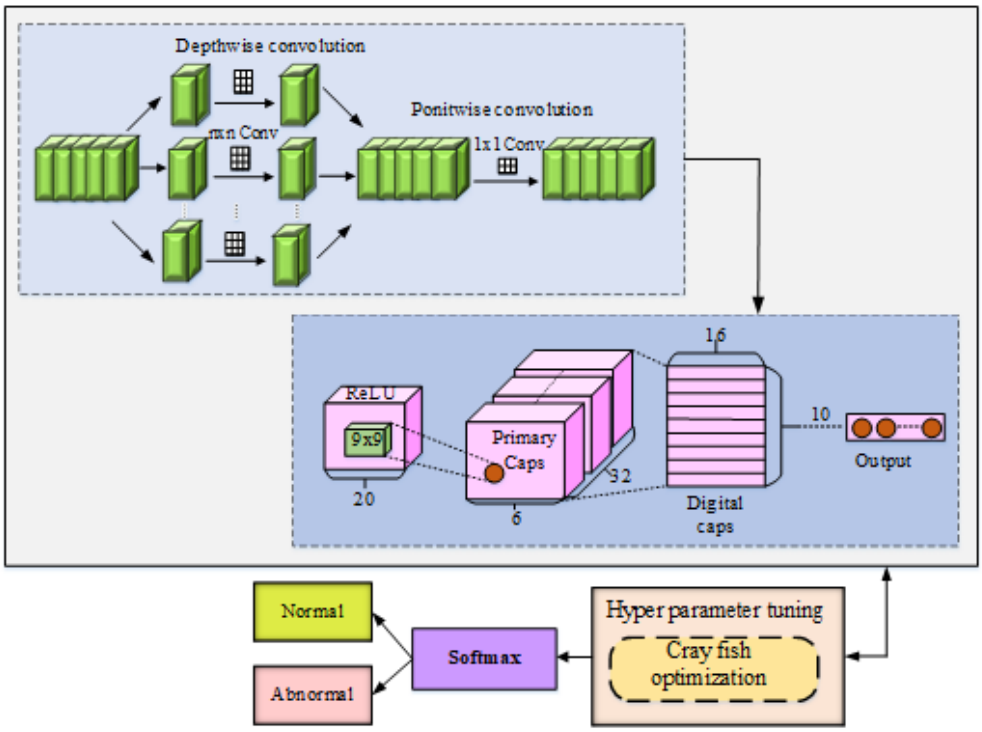

Fig. 5. Architecture of proposed classifier model

Finally, each capsule's output is generated by taking the early path value given by equation (12).

$$u_j = \frac{||u_j||^2}{1+||u_j||^2} \frac{u_j}{||u_j||} \tag{12}$$

here, c_{ij} input vector to the capsule j as well as v_j output. Through the routing mechanism, which is contingent upon an agreement among u_j as well as $u_{j|i}$.

$$b_{ij} = u_j . v_{j|i}. \tag{13}$$

Every capsule k in the last layer is connected to a loss functionl_k. Success is in the losing role l_k is intended.

$$v_k = R_k \, max(0, m^+ - ||u_k||)^2 + \chi(1 - R_k) \, max(0, ||u_k|| - m^-)^2 \tag{14}$$

International Journal of Emerging Research in Engineering, Science, and Management
Vol. 5 | Issue 2 | pp. 01-22 | Apr-Jun 2026.
www.ijeresm.com | eISSN – 2583-4894
Received: 28 Dec 2025 | Revised: 06 Apr 2026 | Accepted: 18 Apr 2026 | Published: 26 Apr 2026

Here v_k is 1 when class k is really current, 0 else terms $m^+, m^-$and λ are hyperparameters selected before the learning process. The suggested tactic tunes hyperparameters using COA [32].

4 Results and Discussion

To forecast chronic kidney disease, this section evaluates both existing and proposed models using Python. Table 1 provides the hyperparameter settings used in the experiments.

Table 1. Hyperparameter details

Hyperparameter	Values
MaxPooling2D Pool Size	2
Epochs	300
Batch Size	32
Conv2D Kernel Size	3
Dense Layer Sizes	128, 64, 32
Loss Function	Categorical cross-entropy
Optimizer	Crayfish Optimization Algorithm
Training and testing ratio	80% and 20%

To ensure reliability and generalization capability, a strict patient-level data splitting strategy was adopted, where all images corresponding to a single patient were assigned exclusively to either the training or testing set, thereby eliminating any possibility of data leakage. In addition, k-fold cross-validation was performed at the patient level to further validate the model's robustness. The high predictive performance can be attributed in part to the integration of multi-scale feature extraction using transfer learning, optimal feature selection through UPSO, and the effective classification capability of the hybrid depth-wise convolutional and deep capsule network. Furthermore, the use of rigorous validation protocols helps ensure that the results obtained reflect improved generalization rather than overfitting.

4.1 Dataset Description

To train and validate the proposed DL model, this study uses benchmark CKD datasets.

4.1.1. CKD Dataset (Dataset-1)

The CT-Kidney Dataset (Normal, Cyst, Tumor, and Stone) [33] is an important medical imaging dataset used for CKD-related classification tasks. It contains 12,446 CT scans of the kidney, categorized into normal kidney, cyst, stone, and tumor. Several hospitals in Dhaka, Bangladesh, assembled the dataset using PACS systems. Regions of interest (ROIs) were systematically extracted from DICOM images for each diagnostic category. Next, the DICOM images were converted into JPEG image format for processing. The classification accuracy of the images was rigorously evaluated by radiologists and medical technicians. There are 12,446 distinct data points in this dataset, counting 3,709 cysts, 5,077 normals, 1,377 stones, and 2,283 tumors contained inside. In this study, normal classes are considered healthy, while cyst, stone, and tumor classes are considered abnormal.

4.1.2. Kidney Intelligent Diagnosis System (KIDS) Dataset (Dataset-2)

The second retinal image dataset used corresponds to the multicenter Kidney Intelligent Diagnosis System (KIDS) cohort described in Wu et al. [34], which includes retinal images collected from multiple hospitals for CKD screening and pathological classification. The KIDS cohort dataset described in [34] includes healthy subjects with a mean age of 26 ± 11 (19–77) years and CKD patients with renal sclerosis with a mean age of 59 ± 14 (19-80) years and a mean CKD stage of 3.5 ± 1.2 (1-5). A total of 2340 images are available, of which 1170 are normal, and 1170 are considered CKD images. From the total dataset, 80% is used for training, and 20% is for testing. Before any preprocessing or feature extraction, the dataset is divided into training and testing sets to avoid training–testing contamination.

Features are created separately for every split, and pretrained CNNs are employed as frozen feature extractors. Only the training data are used for hyperparameter optimisation; the test set is not seen at all until the final assessment. Inception-V3, ResNet-50, and VGG-16 are some of the methods used to extract features from these dataset images. These models extract features from high-dimensional image datasets, such as Inception-V3 and ResNet-50 (2048 features) and VGG-16 (512 features). A total of 4608 features were extracted from the image datasets using feature extraction models. Fig. 6 below shows sample images of high-dimensional medical image data extracted using various feature extraction models.

International Journal of Emerging Research in Engineering, Science, and Management
Vol. 5 | Issue 2 | pp. 01-22 | Apr-Jun 2026.
www.ijeresm.com | eISSN – 2583-4894
Received: 28 Dec 2025 | Revised: 06 Apr 2026 | Accepted: 18 Apr 2026 | Published: 26 Apr 2026

(a) Inception-V3 features

(b) ResNet-50 features

(c) VGG-16 features

Fig. 6. Sample Images of High-dimensional Data Representation

The model is trained using 4608 extracted high-dimensional image features, and the system performance is measured using these features.

4.2. Performance Metrics

Accuracy, precision, and recall are among the performance metrics that are assessed in this area. The effectiveness of the proposed method on the CT kidney dataset was evaluated using the confusion matrix.

International Journal of Emerging Research in Engineering, Science, and Management
Vol. 5 | Issue 2 | pp. 01-22 | Apr-Jun 2026.
www.ijeresm.com | eISSN – 2583-4894
Received: 28 Dec 2025 | Revised: 06 Apr 2026 | Accepted: 18 Apr 2026 | Published: 26 Apr 2026

The main purpose is to determine how many samples were misclassified. The prediction rate of the proposed technique was analyzed based on the forecast and target classes. One or two samples were incorrectly predicted, whereas the other two classes achieved nearly 100% recognition accuracy. In Fig. 7 (a and b), the confusion matrix investigation is revealed. Dataset 1 contains four different classes, whereas 495 images are correctly classified as cyst, whereas 8 images are misclassified as normal, stone, and tumor classes. Similarly, for dataset 2, two classes are considered: normal and sclerosed. 1149 images are correctly classified as normal, and 21 images are misclassified as sclerosed. The confusion matrix is used to assess the overall performance of the proposed framework.

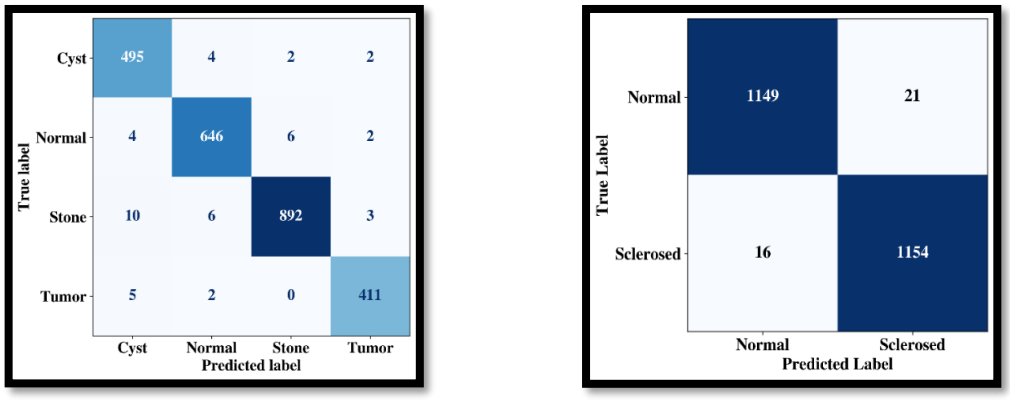

(a) (b)

Fig. 7. Confusion Matrix Analysis

Training accuracy, testing accuracy, training loss, and testing loss of the suggested and prior approaches are shown in Fig. 8 (a-d). During training and testing the dataset, the accuracy and loss of the suggested methods were assessed. The performance of the suggested tactic is examined and compared with other relevant methods to assess its effectiveness. Fig. 8(a) and (b) demonstrate that, compared to alternative comparison approaches, the accuracy is higher while training and evaluating the data. The efficiency of the suggested technique is also shown in Fig. 8(c) and (d), which depict the loss rate when assessing the data using other relevant systems.

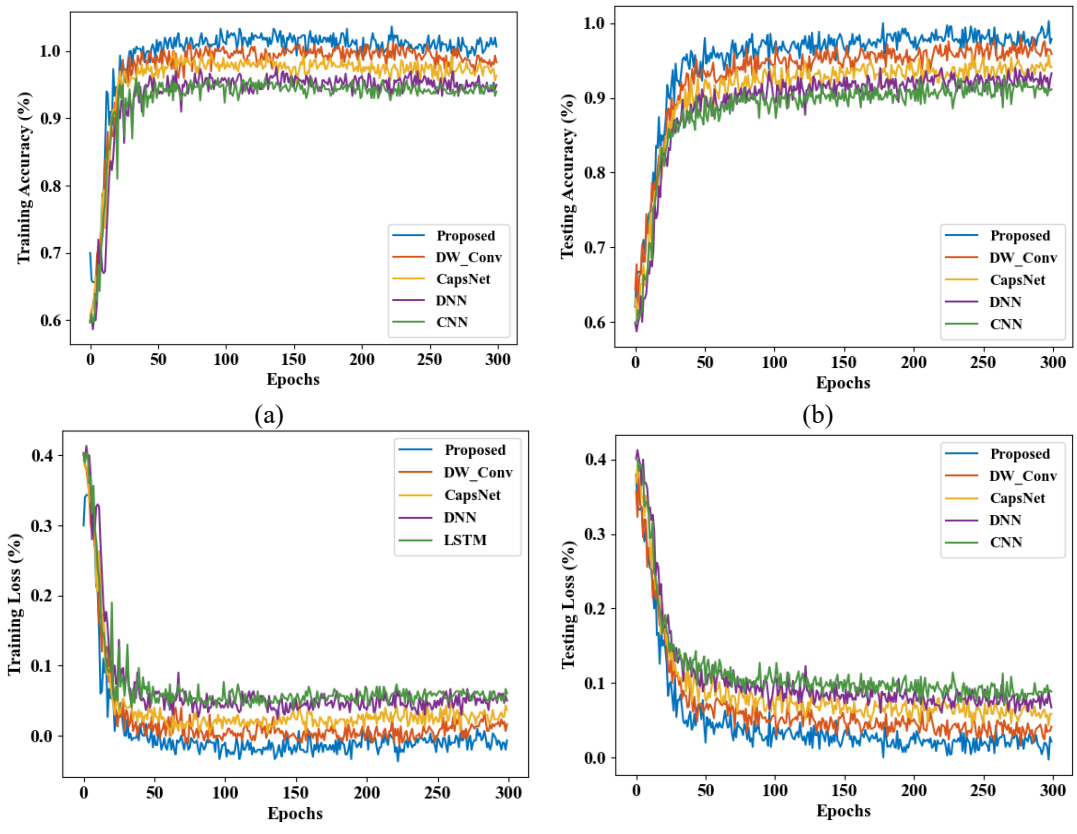

(a) (b)

(c) (d)

Fig. 8. Training and Testing Accuracy and Loss

International Journal of Emerging Research in Engineering, Science, and Management
Vol. 5 | Issue 2 | pp. 01-22 | Apr-Jun 2026.
www.ijeresm.com | eISSN – 2583-4894
Received: 28 Dec 2025 | Revised: 06 Apr 2026 | Accepted: 18 Apr 2026 | Published: 26 Apr 2026

4.2.1. Performance Analysis using Dataset-1

This section describes a graphical representation of each performance metric. The existing models that are compared with the proposed model are CNN, DNN, CapsNet, and DW-Conv. These existing models are implemented and evaluated for comparison. The models follow the same pre-processing and feature extraction models of the proposed framework. The same training and testing data splits are used for both the proposed and comparison models. Fig. 9(a) and 9(b) detail the accuracy and precision performance evaluation.

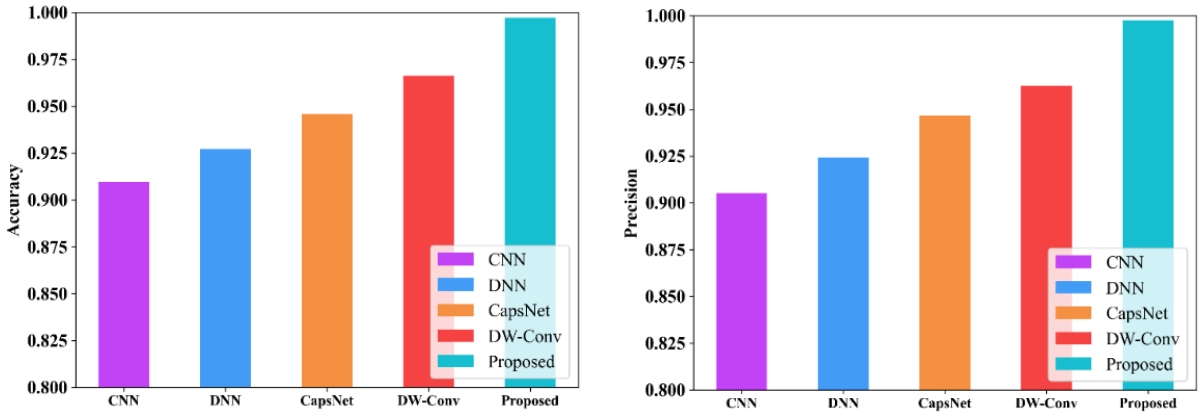

(a) (b)

Fig. 9. Performance Analysis (a) Accuracy and (b) Precision

The plots demonstrate the effectiveness of the proposed classifier in detecting CKD. The accuracy and efficiency of the proposed and current models are contrasted in Fig. 9(a). While existing models have accuracy results below 0.99, the proposed technique has an accuracy result of 0.9972. The precision efficiency of the suggested and prevailing methods is contrasted in Fig. 9(b). While current methods yield values below 0.99, the proposed method achieves a precision value of 0.9966. Fig. 10(a) and 10(b) compare recall and F-measure performance.

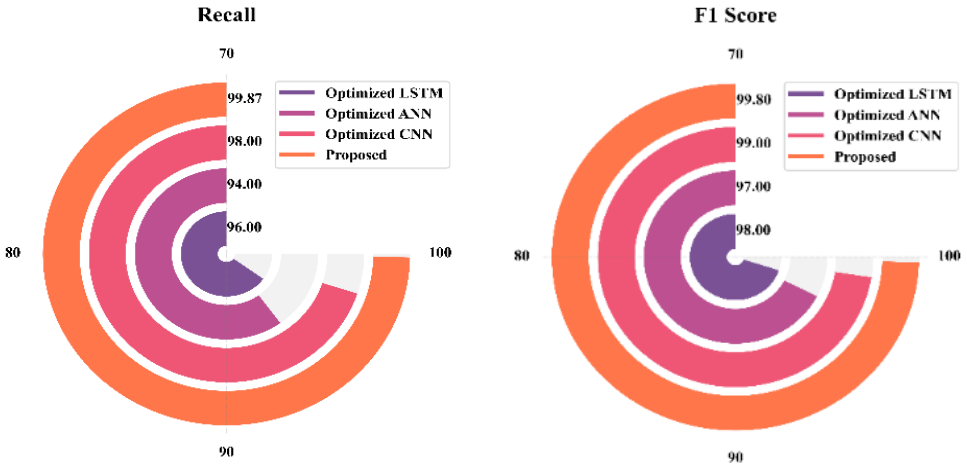

(a) (b)

Fig. 10. Performance Analysis (a) Recall and (b) F1 score

The graphs demonstrate that the proposed approach performs better than competing approaches. The proposed method obtains 0.9976, whereas the other models score less than 0.90, as shown in Fig. 10(a). The suggested approach achieves 0.9971 F1 score outcomes in Fig. 10(b), while other models achieve F1-scores of less than 0.90. MSE and RMSE measures' performance analysis is shown in Fig. 11(a) and 11(b). For both suggested and current models, this graph displays error metrics investigation, such as MSE and RMSE. The suggested method has an RMSE of 0.0347 and an MSE performance of 0.0012. The proposed method achieves lower error values in CKD prediction compared with existing models, as seen by lower error performance. The proposed model is evaluated using additional metrics, such as sensitivity, specificity, and Area under Curve (AUC), as shown in Fig. 12.

International Journal of Emerging Research in Engineering, Science, and Management
Vol. 5 | Issue 2 | pp. 01-22 | Apr-Jun 2026.
www.ijeresm.com | eISSN – 2583-4894
Received: 28 Dec 2025 | Revised: 06 Apr 2026 | Accepted: 18 Apr 2026 | Published: 26 Apr 2026

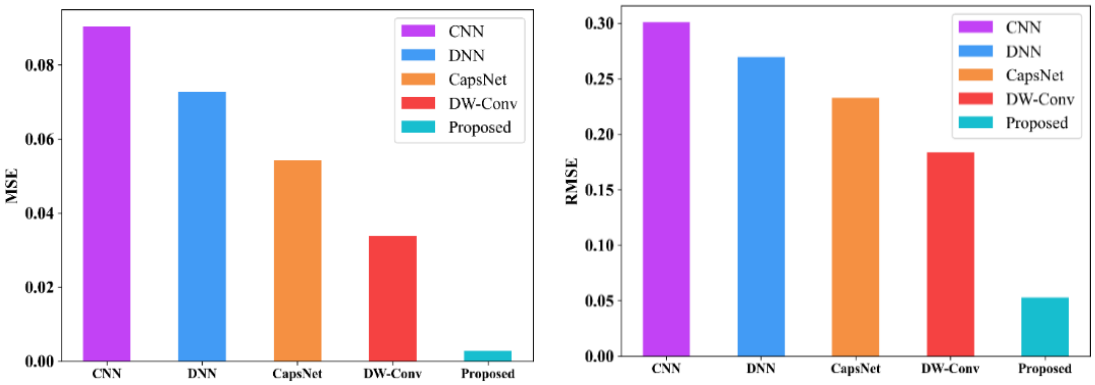

(a) (b)

Fig. 11. Performance Analysis (a) MSE and (b) RMSE

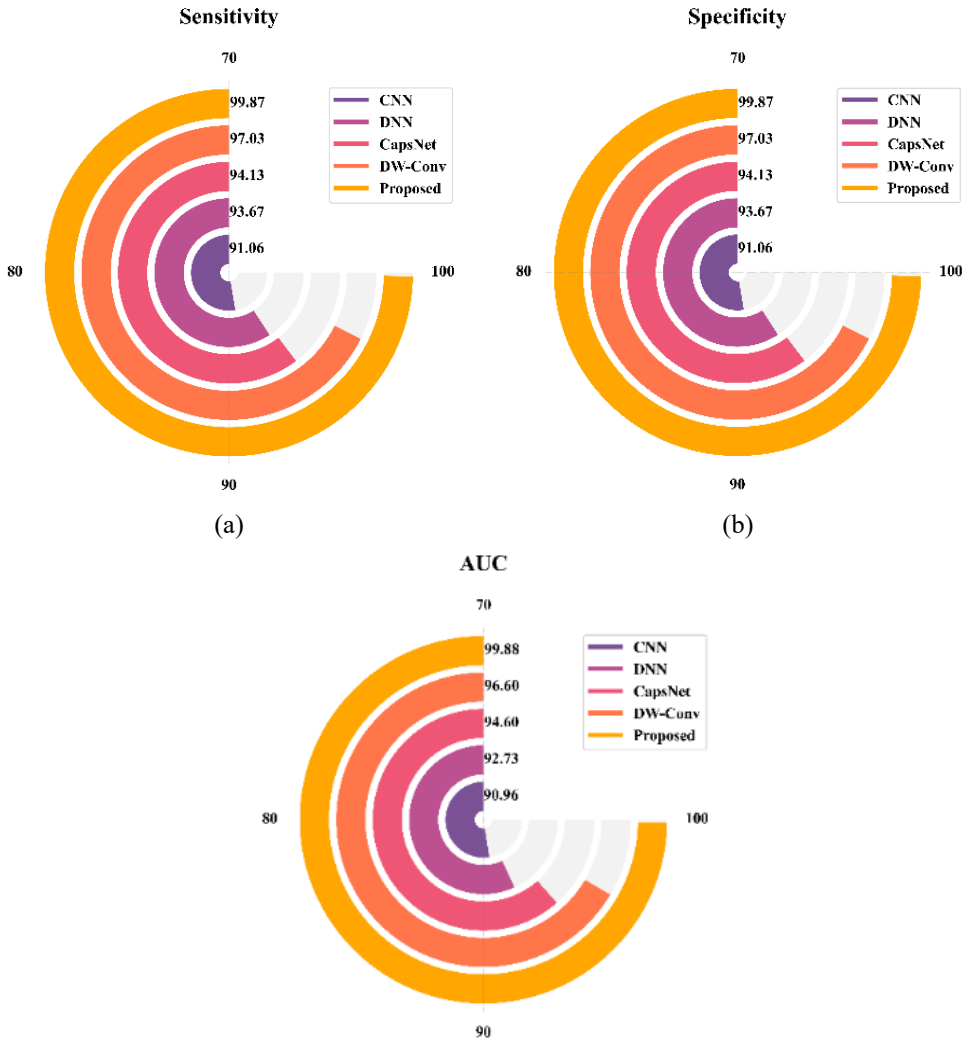

(a) (b)

(c)

Fig. 12. Performance Analysis (a) Sensitivity, (b) Specificity, (c) AUC

The suggested model has a high specificity (0.9985) and sensitivity (0.9987), which means it can accurately find CKD cases while lowering the number of false positives and false negatives. Other models, on the other hand, have lower sensitivity (0.9105–0.9702) and specificity (0.9102–0.9708), which means that they are more likely to make mistakes. While high specificity lowers false alarms and avoids unnecessary follow-up examinations, high sensitivity guarantees fewer missed CKD patients.

International Journal of Emerging Research in Engineering, Science, and Management
Vol. 5 | Issue 2 | pp. 01-22 | Apr-Jun 2026.
www.ijeresm.com | eISSN – 2583-4894
Received: 28 Dec 2025 | Revised: 06 Apr 2026 | Accepted: 18 Apr 2026 | Published: 26 Apr 2026

Advanced feature extraction by Inception-V3, ResNet-50, and VGG-16, as well as optimized classification utilizing depth-wise convolutional networks, is responsible for the suggested model's superior performance. Deep capsule models provide improved feature representation for CKD classification tasks. Additionally, the suggested model achieved a higher AUC of 0.99, demonstrating a balance between true positive and false negative rates. Fig. 13 shows the precision, recall, and F1-score comparisons between the suggested scheme and other models already in use.

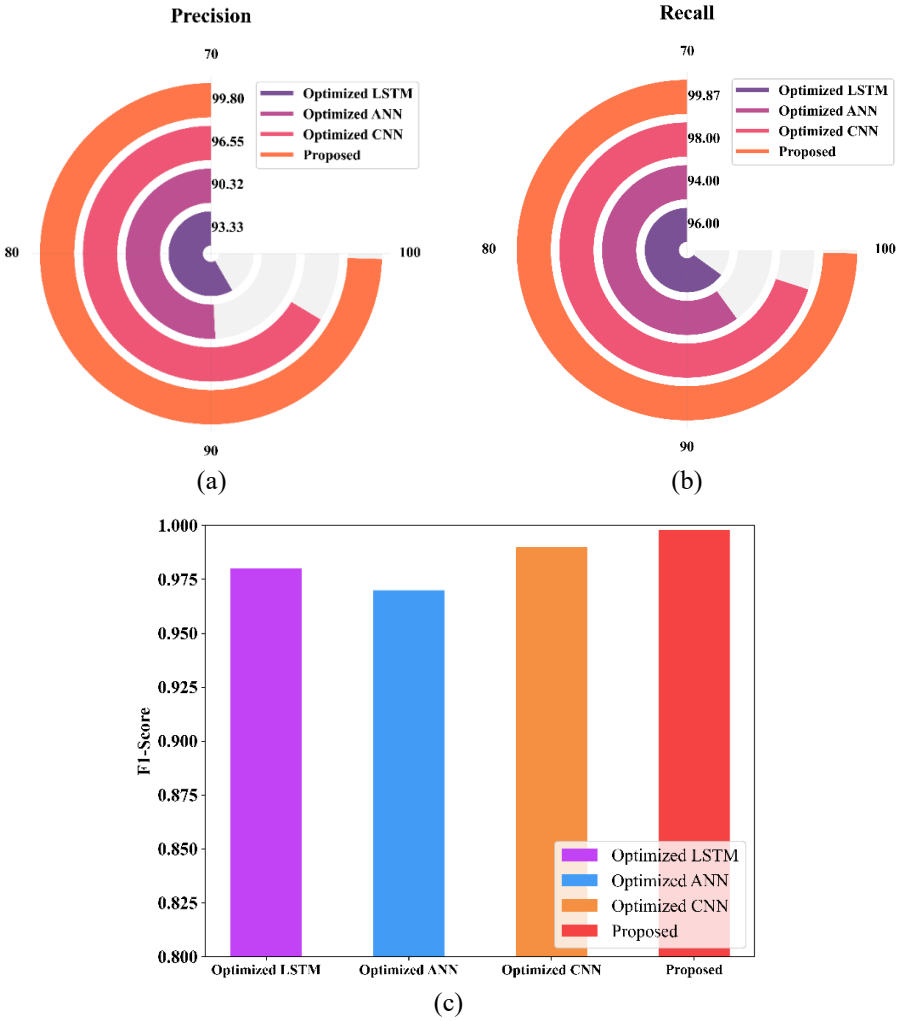

Fig. 13. Performance Evaluation of Proposed Model using (a) Precision, (b) recall, (c) F1-score

The DCN_DC model demonstrates superior performance in CKD prediction, achieving 0.9987 recall, 0.9986 precision, and 0.9988 F1-score, outperforming existing models such as Optimized CNN, which provides 98.75% recall, 98% precision, 99% F1-score, Optimized ANN possesses 96.25% recall, 94% precision, 97% F1-score, and Optimized LSTM achieves 97% recall, 96% precision, and 98% F1-score. The higher recall of the proposed model confirms that fewer CKD cases are missing, while its high precision minimizes false positives, making it suitable for experimental clinical decision-support applications. The hyperparameter and model parameter details for existing models are gathered from [35]. The F1-score of 0.9988 suggests a balance between sensitivity and specificity, thus the detection of CKD is precise.

The proposed DCN_DC model demonstrates improved performance for CKD prediction compared with existing models. These improvements come from the combination of feature selection methods (UPSO), classification strategies (depth-wise convolutional network using deep capsule model), and feature extraction strategies (using Inception-V3, ResNet-50, and VGG-16). In Fig. 14, the proposed model is compared to the existing systems. In a comprehensive model performance evaluation, the proposed model attains an astounding accuracy score of 99.72%, which is superior to both traditional and enhanced deep learning techniques' performance in the prediction of CKD. When compared to the proposed method, the existing methods like Optimized CNN (98.75%), 1-D CorrNN-LSTM (98.08%), and DNN (98%) have relatively good accuracy but are not enough. Although SVM (97.76%), CNN-SVM (96.59%), and EDL-CDSS (96.91%) perform competitively, they are less effective when dealing with complex feature representations. The lower accuracy of ANN-SVM (92.3%) and ANN (88%) models suggested that they cannot sufficiently represent the complex CKD patterns.

International Journal of Emerging Research in Engineering, Science, and Management
Vol. 5 | Issue 2 | pp. 01-22 | Apr-Jun 2026.
www.ijeresm.com | eISSN – 2583-4894
Received: 28 Dec 2025 | Revised: 06 Apr 2026 | Accepted: 18 Apr 2026 | Published: 26 Apr 2026

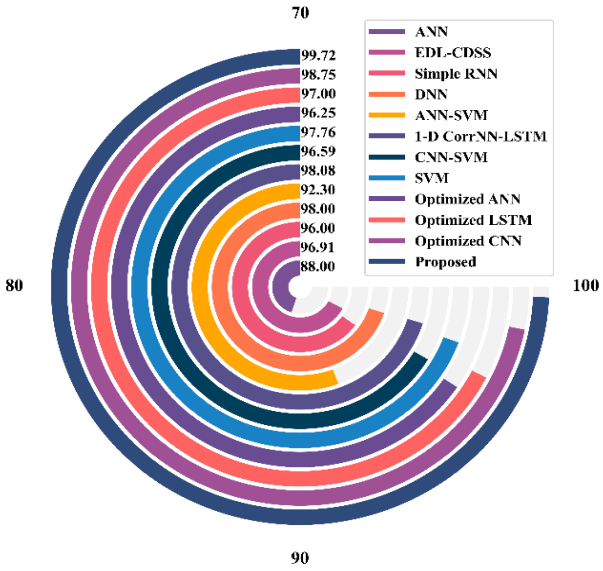

Fig. 14. Comparative analysis of the suggested model

4.2.2. Performance Analysis using Dataset-2

The performance analysis for proposed and existing models using dataset 2 is discussed below. The accuracy, precision, recall, and F1-score analysis are shown in Fig. 15. The existing models that are taken for comparison are DWConv, CapsNet, DNN, and CNN.

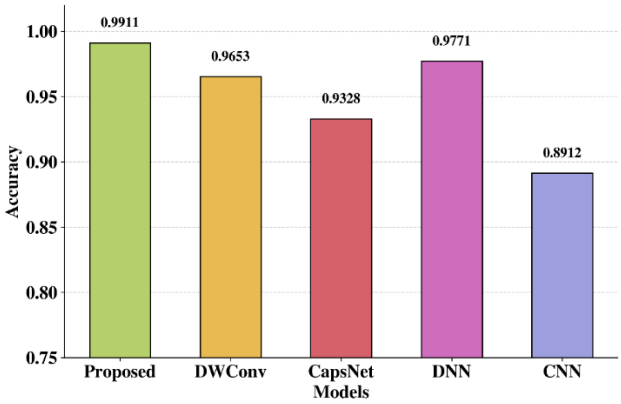

(a) Accuracy

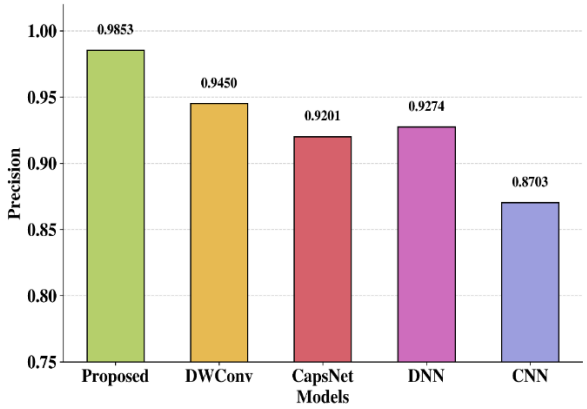

(b) Precision

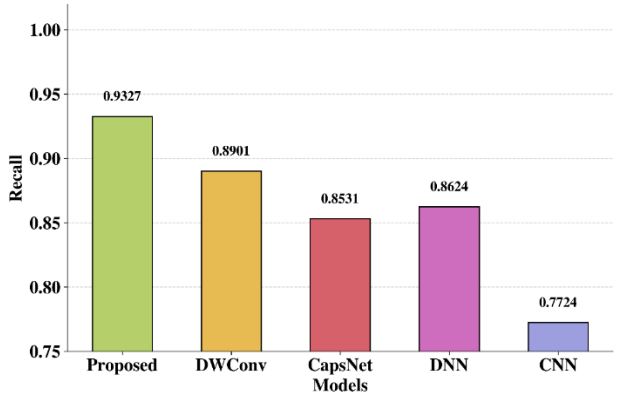

(c) Recall

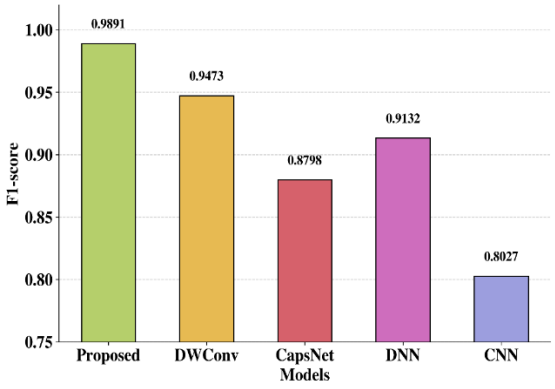

(d) F1-score

Fig. 15. Accuracy, precision, recall, and F1-score analysis

The accuracy, precision, recall, and F1-score analysis for proposed and existing models are shown in Fig. 15. The accuracy, precision, recall, and F1-score of the proposed model are found to be 0.9911, 0.9853, 0.9327, and 0.9891, respectively. The obtained values are found to be better than the compared existing models.

International Journal of Emerging Research in Engineering, Science, and Management
Vol. 5 | Issue 2 | pp. 01-22 | Apr-Jun 2026.
www.ijeresm.com | eISSN – 2583-4894
Received: 28 Dec 2025 | Revised: 06 Apr 2026 | Accepted: 18 Apr 2026 | Published: 26 Apr 2026

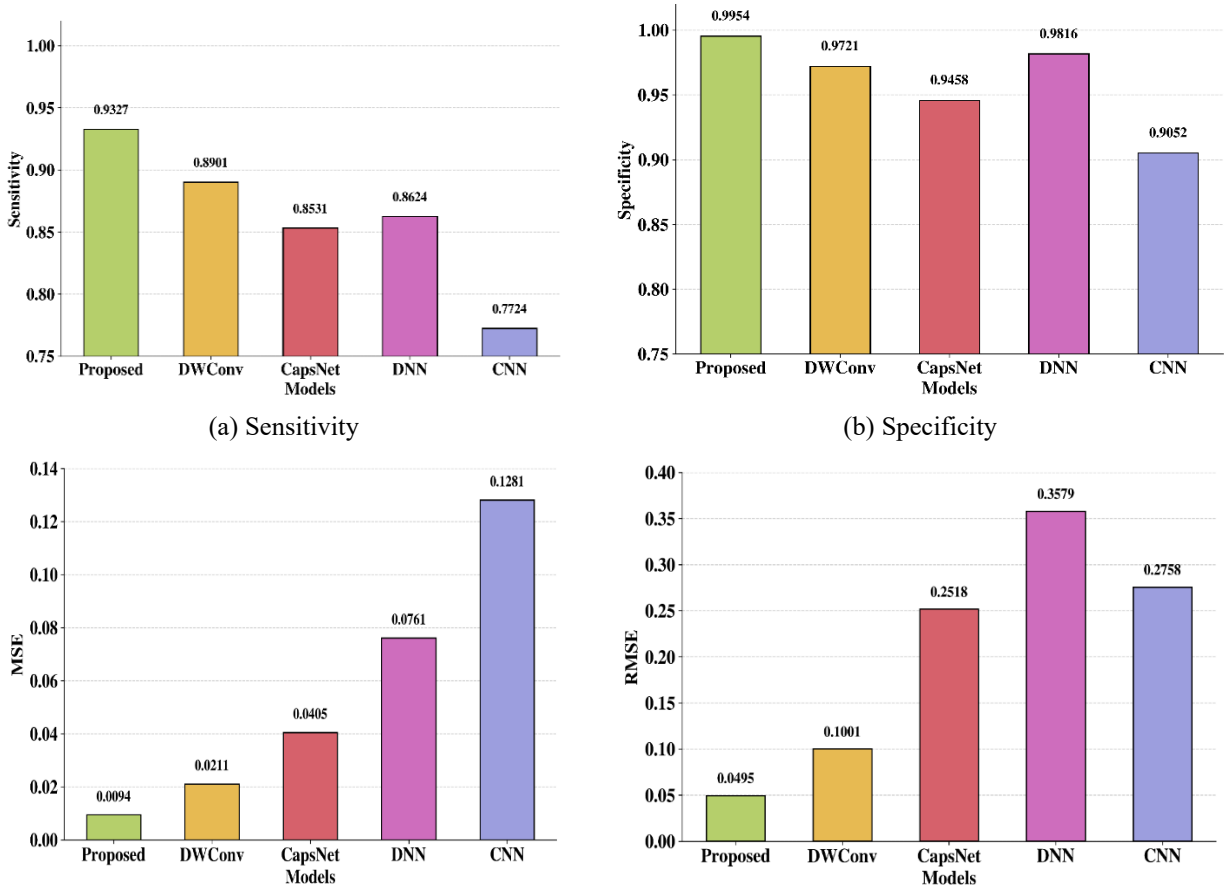

Fig. 16. Sensitivity, Specificity, MSE, and RMSE Analysis

The sensitivity and specificity analysis for proposed and existing models are demonstrated in Fig. 16 (a-b). The sensitivity and specificity for the proposed method are found to be 0.9327 and 0.9954, respectively. The existing models, such as DWConv, CapsNet, DNN, and CNN, have attained a sensitivity value of 0.8901, 0.8531, 0.8624, and 0.7724, respectively. The obtained values are found to be less than the proposed sensitivity value. This is because the proposed model has gathered large features from the input data with less dimensional complexity. This enhances the overall performance of the proposed model over other existing algorithms. The MSE and RMSE performance is illustrated in Fig. 16 (c-d). The MSE and RMSE of the proposed model are found to be 0.0094 and 0.0495, respectively.

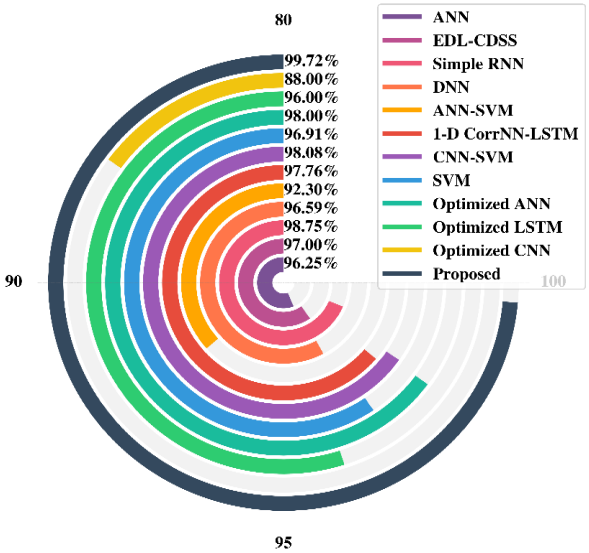

Fig. 17. Accuracy Comparison between Proposed and Existing Models

International Journal of Emerging Research in Engineering, Science, and Management
Vol. 5 | Issue 2 | pp. 01-22 | Apr-Jun 2026.
www.ijeresm.com | eISSN – 2583-4894
Received: 28 Dec 2025 | Revised: 06 Apr 2026 | Accepted: 18 Apr 2026 | Published: 26 Apr 2026

The accuracy comparison between proposed and existing models using dataset 2 is shown in Fig. 17. The existing models, like ANN, EDL-CDSS, simple RNN, DNN, ANN-SVM, 1-D CorrNN-LSTM, CNN-SVM, SVM, optimized ANN, optimized LSTM, optimized CNN, are considered to make a performance comparison with the proposed model.

Table 2. k-fold Validation Analysis with Variance for Datasets 1 and 2

Dataset	Model	Accuracy (%)	Precision (%)	Recall (%)	F1-score (%)	mAP (%)	Kappa	Dice (%)
Dataset- 1	Proposed	99.720 ± 0.1080	95.21 ± 0.1130	99.56 ± 0.122	97.19 ± 0.1718	95.29 ± 0.1351	0.993 ± 0.0007	98.49 ± 0.1321
	UNet	97.65 ± 0.0979	85.31 ± 0.1300	97.97 ± 0.1798	89.73 ± 0.1735	85.27 ± 0.1502	0.967 ± 0.0010	93.31 ± 0.1286
	UNetPP	94.4485 ± 0.1202	76.2085 ± 0.1057	95.5215 ± 0.2084	81.8198 ± 0.0996	76.2230 ± 0.1961	0.9236 ± 0.0011	87.8630 ± 0.1335
	ViT	91.5331 ± 0.1344	70.4699 ± 0.1837	91.6943 ± 0.0945	75.9199 ± 0.1018	70.5151 ± 0.0872	0.8841 ± 0.0010	82.0914 ± 0.0884
	AlexNet	89.2885 ± 0.0949	66.5143 ± 0.1595	88.6000 ± 0.1649	72.0160 ± 0.1859	66.3747 ± 0.1035	0.8541 ± 0.0010	78.4974 ± 0.1812
Dataset-2	Proposed	98.47 ± 0.1801	96.3700 ± 0.1824	99.58 ± 0.2027	97.97 ± 0.2808	96.50 ± 0.217	0.9898 ± 0.0014	99.4453 ± 0.2189
	UNet	97.5200 ± 0.1500	83.1100 ± 0.18	97.61 ± 0.292	89.30 ± 0.258	83.06 ± 0.208	0.934 ± 0.0018	96.34 ± 0.206
	UNetPP	95.1200 ± 0.19	72.5500 ± 0.12	95.2900 ± 0.33	81.20 ± 0.134	72.57 ± 0.237	0.8700 ± 0.002	93.02 ± 0.207
	ViT	92.6600 ± 0.20	64.902 ± 0.198	93.2800 ± 0.14	74.61 ± 0.126	64.95 ± 0.094	0.819 ± 0.001	90.3200 ± 0.13
	AlexNet	89.9900 ± 0.142	58.3000 ± 0.154	89.76 ± 0.2469	68.11 ± 0.2110	58.16 ± 0.100	0.76 ± 0.0016	85.91 ± 0.259

The k-fold validation analysis is shown in Table 2. Instead of doing data partitioning at the image level, it was done at the patient level to prevent any training–testing contamination. To be more precise, during k-fold cross-validation, no single patient's images were ever shared between folds; instead, they were solely allocated to either the training set or the testing set inside a particular fold. The possibility of learning patient-specific anatomical or imaging artifacts, which may otherwise result in falsely inflated performance, is eliminated by using this patient-wise splitting technique to guarantee that the model is tested on patients who have never been seen before. Instead of memorizing subject-specific patterns, the outcomes reported show the model's actual capacity to generalize across other cases. The k-fold validation analysis is performed to show the efficiency of the proposed model on datasets 1 and 2. This illustrates the scalability of the proposed model on different datasets. The proposed technique achieves higher accuracy due in part to the integration of a depth-wise convolutional network with a deep capsule model, Inception-V3, ResNet-50, and VGG-16 for feature extraction, and UPSO for feature selection. These enhancements collectively result in improved feature learning that is easier and more effective. The statistical analysis for proposed and existing models is shown in Table 3. The p-value for the proposed model indicates statistically significant improvement compared with existing models.

Table 3. t-test Analysis Results

Methods	Mean accuracy	Standard deviation	T-statistic	p-value
DWConv	0.9597	0.00149	7.56513	0.00479
CapsNet	0.95439	0.001897	9.19906	0.002716
DNN	0.9478	0.001475	11.48658	0.001416
CNN	0.9407	0.0014944	13.77409	0.0828
Proposed	0.9972	0.00187	2.5652	0.0023

Throughout k-fold cross-validation, the entire performance metrics are reported as mean ± standard deviation with 95% confidence intervals. Robustness analysis shows steady performance enhancement under diverse experimental conditions, and statistical hypothesis analysis shows the improvements are statistically significant for most comparison models ($p < 0.05$). The ablation study results for datasets 1 and 2 are presented in Table 4. This analysis is performed to illustrate the effectiveness of each model on the proposed framework. The pre-processing has the ability to enhance the overall classification performance. For feature extraction, Inception-V3, ResNet-50, and VGG-16 are used, which take advantage of the models' complementary strengths. Inception-V3 uses parallel convolutional paths to generate multi-scale feature representations, VGG-16 obtains fine-grained spatial textures, and ResNet-50 applies residual learning to extract deep semantic features with better stability. Robustness and discrimination are enhanced with a combination of these heterogeneous features, especially for images with structures of different contrasts and sizes.

International Journal of Emerging Research in Engineering, Science, and Management
Vol. 5 | Issue 2 | pp. 01-22 | Apr-Jun 2026.
www.ijeresm.com | eISSN – 2583-4894
Received: 28 Dec 2025 | Revised: 06 Apr 2026 | Accepted: 18 Apr 2026 | Published: 26 Apr 2026

Table 4. Ablation Study Analysis

Model	Dataset-1 Accuracy (%)	Dataset-2 Accuracy (%)
Without MMG	94.54	92.44
Without CLAHE	95.7	94.28
Without Inception-V3	97.85	96.92
Without ResNet-50	98.42	97.58
Without VGG-16	95.96	94.87
Without UPSO	96.88	95.94
Without Deep Capsule Networks	97.63	96.71
Without Depth-wise CNNs	96.41	95.36
Proposed	**99.72**	**98.47**

The dimensionality issue of extracted features is successfully reduced using the UPSO algorithm. This component contributes to reducing the overall complexity of the proposed framework. Finally, the classification models, deep capsule networks, depth-wise CNNs, and COA are integrated, which enhances the complementary strengths of the integrated models. Capsule networks maintain spatial and hierarchical links between features, depth-wise CNNs offer computationally efficient feature learning, and COA intelligently chooses features and hyperparameters to increase classification accuracy, resilience, and generalization. The usage of each model depicts its own contribution, which is beneficial to enhance the overall performance of the proposed model on CKD classification.

4.2.3. Computational Costs and Resource Requirements

The proposed method requires significant computational resources because it combines several DL models (Inception-V3, ResNet-50, and VGG-16) for feature extraction, a depth-wise convolutional network with a deep capsule model, and a UPSO technique. Training DL models on high-dimensional medical image datasets is computationally intensive, especially because of the high-dimensional feature extraction procedure and COA-based hyperparameter optimization. The model was trained on a high-performance computing system with GPU support to handle computational complexity efficiently. The 4,608-dimensional feature vectors that need to be managed during the feature extraction stage alone increase processing time and memory consumption.

Furthermore, the depth-wise convolutional network and capsule network need a lot of processing resources due to their complex hierarchical representations and dynamic routing strategies. Despite these processing demands, depth-wise convolutions outperform old CNNs in terms of efficiency by utilizing fewer parameters. This method is still challenging to apply in resource-constrained scenarios, such as mobile health apps or real-time clinical settings. Future studies should focus on model compression techniques like pruning, quantization, and knowledge distillation to lower processing costs without sacrificing accuracy. Furthermore, using a lightweight version of the model for edge computing devices should enable real-time CKD prediction in resource-constrained healthcare settings.

4.3. Discussion

The performance of the proposed method was evaluated against numerous similar approaches to assess its effectiveness. According to the evaluation, the recommended method effectively avoids the drawbacks of earlier research, such as subpar performance, extensive processing, a small dataset, and so on. The integrated filtering and histogram equalization successfully decrease noise and increase visual contrast, making the input to the model cleaner and more informative. Pre-trained methods (such as Inception-V3, ResNet-50, and VGG-16) are utilized to effectively extract high-level visual features to reduce training time and potentially increase accuracy. While dimensionality and computing costs are reduced by employing an enhanced UPSO procedure to select the most useful features, the model stays focused on relevant data. By merging the powerful representational abilities of capsule networks with the efficiency of depth-wise convolutions, the proposed depth-wise convolutional network with a deep capsule model effectively captures intricate visual patterns. The proposed and prevailing methods are contrasted in Table 5.

Table 5. Accuracy Comparison of the Proposed Method with the State-of-the-art Methods

Methods	Dataset	Accuracy (%)
HMANN [17]	CKD dataset	97.5
H-DKN [18]	TCIA-based CKD dataset	97
LSTM [20]	UCI ML repository dataset	83
GNN and Tabular Data Model [21]	UCI ML repository dataset	95.089
DNN [22]	UCI ML repository dataset	97
Proposed	CT Kidney dataset and KIDS dataset	**99.72, and 99.11**

International Journal of Emerging Research in Engineering, Science, and Management
Vol. 5 | Issue 2 | pp. 01-22 | Apr-Jun 2026.
www.ijeresm.com | eISSN – 2583-4894
Received: 28 Dec 2025 | Revised: 06 Apr 2026 | Accepted: 18 Apr 2026 | Published: 26 Apr 2026

According to the experimental results, the proposed system achieves better predictive performance in CKD detection than existing DL strategies. Using the feature extraction method of Inception-V3, ResNet-50, and VGG-16, the feature extraction combination method guarantees that the extracted features can represent the kidney images sufficiently and reliably. Furthermore, the efficiency of selecting the most discriminative features from the pool of features is enhanced by using the UPSO, which leads to enhanced classification accuracy with reduced computational cost at the same time. Deep capsule models and depth-wise convolutional networks are jointly employed to bring a powerful mechanism to capture complex spatial relationships and hierarchical structures in the medical image. The proposed model achieves a high accuracy of 99.72% in the CKD classification, which is much better than existing techniques such as CNN (92%) and GNN (95.08%). By selecting features in an optimal way, the UPSO algorithm enhances the generalization of the model and removes redundant information.

In particular, the COA is trained to tune the model's parameters to yield faster convergence and stability. In comparison with traditional deep learning models, depth-wise convolution reduces the number of parameters and greatly improves the efficiency of models, and accelerates training time. Clinically selected renal images with well-defined diagnostic labels are included in both datasets. Pathological patterns, such as structural anomalies, textural changes, and form distortions, may be easily identified. In contrast to more diverse, multi-organ datasets, kidney-specific datasets are more targeted, which lowers intra-class ambiguity and promotes trustworthy feature learning. For kidney disease characterization, spatial hierarchies and part-whole interactions are crucial, and the deep capsule model excels at capturing them.

Capsule representations allow the model to distinguish minute pathological alterations that traditional convolutional networks would miss by maintaining the posture, orientation, and spatial consistency of kidney structures. Then, by learning channel-wise discriminative patterns and greatly lowering parameter redundancy, the incorporation of a depth-wise convolutional network improves feature extraction efficiency. This architectural decision enhances generalization, prevents overfitting, and enables the model to concentrate on the prominent kidney borders and textures found in both datasets.

4.3.1. Limitations and Future Considerations

The proposed strategy works extremely well but has several shortcomings. The model was trained on a publicly available dataset and, therefore, might not realistically reflect the variety of real-world clinical situations. Further investigations into other demographic and geographic data are suggested for further studies. Even if the proposed model has a high accuracy rate, explainability remains a challenge. Future research can adopt techniques to generate explainable AI (XAI), such as Grad-CAM and SHAP, to assist the decisions of medical professionals and offer increased transparency on models and predictions. The results show that the proposed deep learning strategy with big data is better than current methods in CKD prediction. However, the identified limitations need to be addressed to increase real-world applicability and ensure wider acceptance of the presented method in clinical practice.

Bias in the data fed into an AI-driven healthcare solution can have a great influence on their generalizability. Because the data used in the present study are insufficiently representative of different ethnicities, medical conditions, or clinical settings, predictions may be biased. Robustness may also be affected by differences in the technology used to provide imaging and data collection methods from hospital to hospital. This could be addressed in the future by validating the model on data from several institutions and employing domain adaptation approaches to improve performance across demographics. In addition, motion blur, low contrast, and non-uniform acquisition conditions also affect feature extraction, which brings noise and quality overshooting of the image.

Furthermore, adversarial training and data augmentation are methods that should be explored in future studies to attempt to restore the robustness of the model when developing discrepancies in real-world imaging, even when pre-processing techniques improve the visibility of the images. Even though the proposed approach works well in controlled experiments, it is not yet understood whether it is clinically applicable. The results presented are based on patient-level cross-validation and retrospective evaluation with a single curated dataset. Notwithstanding the promising outcomes, the current study does not assert immediate clinical readiness and is restricted to experimental validation. Future research will concentrate on prospective clinical investigations and an extensive, multi-institutional assessment.

4.4. Implications for Clinical Practice

The traditional blood and urine tests that are used for the diagnosis of CKD may not be accessible in rural or undeveloped areas. The proposed deep learning model trained on kidney images can be applied as a non-invasive automatic diagnostic tool to help doctors detect CKD in an early stage. In the early stages of the disease, it can be prevented, and patient outcome can be positively affected by timely therapy. With an accuracy of 99.72%, the proposed method has fewer false positives and false negatives and provides higher accuracy compared to many other existing diagnostic methods. This could limit the occurrence of misdiagnosis and ensure that CKD patients are provided with proper care in a timely manner. Healthcare personnel are often tasked with handling large amounts of medical imaging data, so manual diagnosis is time-consuming and subject to human error.

International Journal of Emerging Research in Engineering, Science, and Management
Vol. 5 | Issue 2 | pp. 01-22 | Apr-Jun 2026.
www.ijeresm.com | eISSN – 2583-4894
Received: 28 Dec 2025 | Revised: 06 Apr 2026 | Accepted: 18 Apr 2026 | Published: 26 Apr 2026

The suggested model is very accurate and efficient, but some obstacles cannot be ignored before deploying it on a large scale in clinical settings. AI-powered medical tools should be in line with the FDA, CE, and HIPAA regulations to safeguard the safety and data privacy of patients. Many times, clinicians need to know the model's prediction process, and to do that, they will need XAI answers. Further work can be done in the direction of interpretation methods such as SHAP or Grad-CAM. Deployment of an AI-driven model in hospitals involves integration with the existing EHR systems seamlessly, which would need changes in workflow and IT infrastructure. Although the suggested approach presented encouraging results, its clinical implementation would necessitate multi-center validation, rigorous data governance (HIPAA (Health Insurance Portability and Accountability Act of 1996)/GDPR (General Data Protection Regulation)), regulatory framework compliance (e.g., FDA - Food and Drug Administration, MDR - medical device regulation), and smooth interaction with current clinical workflows. Future translational research must address these important issues.

5 Conclusions

This study proposed a unique way for CKD forecasting that makes use of both DL techniques and image analysis. The superiority of the input data for further analysis was improved by using adaptive histogram equalization in conjunction with mean, median, and Gaussian filtering to efficiently eliminate noise and improve image contrast. It was possible to efficiently extract pertinent picture features by using pre-trained models, which sped up the model training process. The most discriminative features were successfully found using an upgraded PSO approach, which decreased dimensionality and enhanced model performance. A hybrid model that integrated depth-wise convolutional networks and deep capsule models was created to manage complex feature connections and capture detailed visual patterns. The model's weights and parameters were successfully modified by the COA, increasing prediction accuracy. The suggested model achieves 99.72% accuracy compared with existing methods in comparison to the current methods. Class imbalance, which happens when one cluster of data significantly outnumbers the other, is a common problem in CKD datasets. Models that prioritize the majority class may arise from this imbalance, making accurate forecasts impossible. Future research on managing unbalanced data will be carried out using strategies like cost-sensitive learning and synthetic data generation to overcome this difficulty.

FUNDING INFORMATION

This research received no specific grant from any funding agency in the public, commercial, or not-for-profit sectors.

ETHICS STATEMENT

This study did not involve human or animal subjects and, therefore, did not require ethical approval.

STATEMENT OF CONFLICT OF INTERESTS

The authors declare no conflicts of interest related to this study.

References

[1] V. Singh, V. K. Asari, and R. Rajasekaran, “A deep neural network for early detection and prediction of chronic kidney disease,” *Diagnostics*, vol. 12, no. 1, p. 116, Jan. 2022, doi: 10.3390/diagnostics12010116.

[2] K. Zhang *et al.*, “Deep-learning models for the detection and incidence prediction of chronic kidney disease and type 2 diabetes from retinal fundus images,” *Nature Biomedical Engineering*, vol. 5, no. 6, pp. 533–545, Jun. 2021, doi: 10.1038/s41551-021-00745-6.

[3] C. Sabanayagam *et al.*, “A deep learning algorithm to detect chronic kidney disease from retinal photographs in community-based populations,” *The Lancet Digital Health*, vol. 2, no. 6, pp. e295–e302, May 2020, doi: 10.1016/s2589-7500(20)30063-7.

[4] D. A. Debal and T. M. Sitote, “Chronic kidney disease prediction using machine learning techniques,” *Journal of Big Data*, vol. 9, no. 1, Nov. 2022, doi: 10.1186/s40537-022-00657-5.

[5] S. M. M. Elkholy, A. Rezk and A. A. E. F. Saleh, "Early Prediction of Chronic Kidney Disease Using Deep Belief Network," in *IEEE Access*, vol. 9, pp. 135542-135549, 2021, doi: 10.1109/ACCESS.2021.3114306.

[6] W. Wang, G. Chakraborty, and B. Chakraborty, “Predicting the risk of chronic kidney disease (CKD) using machine learning algorithm,” *Applied Sciences*, vol. 11, no. 1, p. 202, Dec. 2020, doi: 10.3390/app11010202.

[7] Q. Bai, C. Su, W. Tang, and Y. Li, “Machine learning to predict end stage kidney disease in chronic kidney disease,” *Scientific Reports*, vol. 12, no. 1, p. 8377, May 2022, doi: 10.1038/s41598-022-12316-z.

[8] E. N. Yildiz, E. Cengil, M. Yildirim, and H. Bingol, “Diagnosis of chronic kidney disease based on CNN and LSTM,” *Acadlore Transactions on AI and Machine Learning*, vol. 2, no. 2, pp. 66–74, Jun. 2023, doi: 10.56578/ataiml020202.

[9] R. Sawhney, A. Malik, S. Sharma, and V. Narayan, “A comparative assessment of artificial intelligence models used for early prediction and evaluation of chronic kidney disease,” *Decision Analytics Journal*, vol. 6, p. 100169, Jan. 2023, doi: 10.1016/j.dajour.2023.100169.

International Journal of Emerging Research in Engineering, Science, and Management
Vol. 5 | Issue 2 | pp. 01-22 | Apr-Jun 2026.
www.ijeresm.com | eISSN – 2583-4894
Received: 28 Dec 2025 | Revised: 06 Apr 2026 | Accepted: 18 Apr 2026 | Published: 26 Apr 2026

[10] S. Krishnamurthy *et al.*, "Machine learning prediction models for chronic kidney disease using national health insurance claim data in Taiwan," *Healthcare*, vol. 9, no. 5, p. 546, May 2021, doi: 10.3390/healthcare9050546.

[11] P. Chittora *et al*., "Prediction of Chronic Kidney Disease - A Machine Learning Perspective," in *IEEE Access*, vol. 9, pp. 17312-17334, 2021, doi: 10.1109/ACCESS.2021.3053763.

[12] K. Nagawa *et al.*, "Three-dimensional convolutional neural network-based classification of chronic kidney disease severity using kidney MRI," *Scientific Reports*, vol. 14, no. 1, p. 15775, Jul. 2024, doi: 10.1038/s41598-024-66814-3.

[13] D. Saif, A. M. Sarhan, and N. M. Elshennawy, "Early prediction of chronic kidney disease based on ensemble of deep learning models and optimizers," *Journal of Electrical Systems and Information Technology*, vol. 11, no. 1, Apr. 2024, doi: 10.1186/s43067-024-00142-4.

[14] A. A. Malibari, "An efficient IoT-Artificial intelligence-based disease prediction using lightweight CNN in healthcare system," *Measurement Sensors*, vol. 26, p. 100695, Feb. 2023, doi: 10.1016/j.measen.2023.100695.

[15] S. A. Hannan and P. Pal, "Detection and classification of kidney disease using convolutional neural networks," *Journal of Neurology and Neurorehabilitation Research*, vol. 8, no. 2, pp. 1-7, 2023, doi: 10.35841/aajnnr-8.2.136.

[16] K. Inoue *et al.*, "The utility of automatic segmentation of kidney MRI in chronic kidney disease using a 3D convolutional neural network," *Scientific Reports*, vol. 13, no. 1, p. 17361, Oct. 2023, doi: 10.1038/s41598-023-44539-z.

[17] F. Ma, T. Sun, L. Liu, and H. Jing, "Detection and diagnosis of chronic kidney disease using deep learning-based heterogeneous modified artificial neural network," *Future Generation Computer Systems*, vol. 111, pp. 17–26, Apr. 2020, doi: 10.1016/j.future.2020.04.036.

[18] V. Nallarasan, V. Ponnusamy, R. Lakshminarayanan, S. k, S. Vigneshwari and R. Vinoth, "Prediction of Kidney Disease Utilizing a Hybrid Deep Learning Methodology," *2024 2nd International Conference on Computer, Communication and Control (IC4)*, Indore, India, 2024, pp. 1-8, doi: 10.1109/IC457434.2024.10486786.

[19] B. S. Lakshmi, V. Anand R, H. Omotunde, M. Birundadevi, M. S and M. G. Brahmam, "Deep Learning for Automated Classification of Kidney Lesions in Chronic Kidney Disease Patients," *2024 International Conference on Integrated Circuits and Communication Systems (ICICACS)*, Raichur, India, 2024, pp. 1-6, doi: 10.1109/ICICACS60521.2024.10498835.

[20] C. Yun *et al.*, "Construction of risk prediction model of Type 2 diabetic kidney disease based on deep learning," *Diabetes & Metabolism Journal*, vol. 48, no. 4, pp. 771–779, Apr. 2024, doi: 10.4093/dmj.2023.0033.

[21] P. K. Rao, S. Chatterjee, K. Nagaraju, S. B. Khan, A. Almusharraf, and A. I. Alharbi, "Fusion of graph and tabular deep learning models for predicting chronic kidney disease," *Diagnostics*, vol. 13, no. 12, p. 1981, Jun. 2023, doi: 10.3390/diagnostics13121981.

[22] H. Kriplani, B. Patel, and S. Roy, "Prediction of chronic kidney diseases using deep artificial neural network technique," in *Lecture Notes in Computational Vision and Biomechanics*, 2019, pp. 179–187. doi: 10.1007/978-3-030-04061-1_18.

[23] J. Yang, S. Rahardja, and P. Fränti, "Mean-shift outlier detection and filtering," *Pattern Recognition*, vol. 115, p. 107874, Feb. 2021, doi: 10.1016/j.patcog.2021.107874.

[24] S. Ramesh, S. Sasikala, and N. Paramanandham, "Segmentation and classification of brain tumors using modified median noise filter and deep learning approaches," *Multimedia Tools and Applications*, vol. 80, no. 8, pp. 11789–11813, Jan. 2021, doi: 10.1007/s11042-020-10351-4.

[25] S. Jayachitra and A. Prasanth, "Multi-Feature analysis for automated brain stroke classification using weighted Gaussian Naïve Bayes Classifier," *Journal of Circuits Systems and Computers*, vol. 30, no. 10, p. 2150178, Dec. 2020, doi: 10.1142/s0218126621501784.

[26] S. Roy, K. Bhalla, and R. Patel, "Mathematical analysis of histogram equalization techniques for medical image enhancement: a tutorial from the perspective of data loss," *Multimedia Tools and Applications*, vol. 83, no. 5, pp. 14363–14392, Jul. 2023, doi: 10.1007/s11042-023-15799-8.

[27] M. Mujahid, F. Rustam, R. Álvarez, J. L. V. Mazón, I. De La Torre Díez, and I. Ashraf, "Pneumonia Classification from X-ray Images with Inception-V3 and Convolutional Neural Network," *Diagnostics*, vol. 12, no. 5, p. 1280, May 2022, doi: 10.3390/diagnostics12051280.

[28] M. Elpeltagy and H. Sallam, "Automatic prediction of COVID− 19 from chest images using modified ResNet50," *Multimedia Tools and Applications*, vol. 80, no. 17, pp. 26451–26463, May 2021, doi: 10.1007/s11042-021-10783-6.

[29] S. K. Betha and J. B. Seventline, "Automated Detection of Diabetic Retinopathy Segmented Images using ResNet50 and VGG16 Deep Learning Algorithms," *2024 Second International Conference on Inventive Computing and Informatics (ICICI)*, Bangalore, India, 2024, pp. 159-165, doi: 10.1109/ICICI62254.2024.00036.

[30] A. G. Gad, "Particle Swarm Optimization Algorithm and its Applications: A Systematic review," *Archives of Computational Methods in Engineering*, vol. 29, no. 5, pp. 2531–2561, Apr. 2022, doi: 10.1007/s11831-021-09694-4.

[31] J. Lu, L. Tan, and H. Jiang, "Review on Convolutional Neural Network (CNN) Applied to Plant Leaf Disease Classification," *Agriculture*, vol. 11, no. 8, p. 707, Jul. 2021, doi: 10.3390/agriculture11080707.

International Journal of Emerging Research in Engineering, Science, and Management
Vol. 5 | Issue 2 | pp. 01-22 | Apr-Jun 2026.
www.ijeresm.com | eISSN – 2583-4894
Received: 28 Dec 2025 | Revised: 06 Apr 2026 | Accepted: 18 Apr 2026 | Published: 26 Apr 2026

[32] H. Jia, H. Rao, C. Wen, and S. Mirjalili, "Crayfish optimization algorithm," *Artificial Intelligence Review*, vol. 56, no. S2, pp. 1919–1979, Sep. 2023, doi: 10.1007/s10462-023-10567-4.

[33] Md Nazmul Islam and Md Humaion Kabir Mehedi, "CT KIDNEY DATASET: Normal-Cyst-Tumor and Stone," Nov. 01, 2021. https://www.kaggle.com/datasets/nazmul0087/ct-kidney-dataset-normal-cyst-tumor-and-stone. Accessed: 10 Dec 2025.

[34] Q. Wu *et al.*, "A noninvasive model for chronic kidney disease screening and common pathological type identification from retinal images," *Nature Communications*, vol. 16, no. 1, p. 6962, Jul. 2025, doi: 10.1038/s41467-025-62273-0.

[35] C. Mondol *et al.*, "Early Prediction of Chronic Kidney Disease: A comprehensive performance analysis of deep learning models," *Algorithms*, vol. 15, no. 9, p. 308, Aug. 2022, doi: 10.3390/a15090308.